Surface dynamics of NaCl(001) by inelastic He atom scattering

S. A. Safron, W. P. Brug, G. Chern, J. Duan, and J. G. Skofronick,
Departments of Chemistry and Physics and MARTECH, The Florida State University, Tallahassee, Florida 32306-3006

J. R. Manson
Department of Physics and Astronomy, Clemson University, Clemson, South Carolina 29634

(Received 7 August 1989; accepted 25 September 1989)

The relatively simple structure of alkali halide crystals has made these materials the paradigm for the understanding of the dynamics of ionic insulators. We have employed a time-of-flight (TOF) technique to determine the energy loss/gain due to single phonon creation/annihilation events in the scattering of He atoms from the NaCl(001) surface. From these data the surface dispersion curves over the $\overline{\Gamma}\overline{M}$ region of the surface Brillouin zone have been constructed. The results compare favorably with both the slab dynamics and the Green's function calculations reported for this crystal, and with previous measurements in the ⟨100⟩ direction. Of particular interest, we report the first evidence for the crossing mode in the ⟨100⟩ direction, which had been predicted for NaCl. Additionally, we have employed the TOF technique to examine the Debye-Waller attenuation of the *elastic* (specular) intensity and the relative height of an *inelastic* multiphonon "foot" at the base of the specular beam as a function of the crystal surface temperature (120–670 K).

I. INTRODUCTION

The surface phonon dispersion curves of a number of alkali halide crystals have been determined by high-resolution He atom scattering.[1-7] This technique is very well suited to these materials because of their low vibrational frequencies and because they are insulators. The momentum and energy of the He atoms can be adjusted to probe the momenta and energies of the surface phonons with a resolution of about $\pm$ 0.2 meV, and the atoms do not penetrate or charge the surface. The alkali halides, in turn, represent model systems for the broad class of compounds of ionic insulators, many of which have important technological uses. For example, the perovskites $SrTiO_3$, $BaTiO_3$, and $LiNbO_3$ are in great demand by the opto-electronic industry, and the ceramics MgO and the new high-temperature superconductors may have important catalytic, mechanical, and electrical properties.

A number of theoretical calculations of the alkali halide surface dispersion curves have been carried out and actually predate the experiments.[8-11] These calculations rely on the shell models to characterize the closed-shell electronic configurations of the ions, an approach that has worked very well with the bulk dispersion curves. Because of their general successes, now with surface vibrations as well, efforts are being made to extend them to the more complicated ionic materials.[12]

One area of surface dynamics which has not received much experimental or theoretical attention is that of multiphonon atom-surface interactions. It has long been understood that as the crystal temperature is raised, the elastic scattering intensity is decreased due to the vibrational displacements from the equilibrium atomic lattice sites; namely, the intensities are attenuated by the Debye-Waller factor.[13] (This applies to x-ray, neutron, electron, and atom/molecule scattering alike.) This attenuation factor applies equally well to the single-phonon creation and annihilation scattering intensities in the high-resolution He scattering experiments.[14] As the temperature is raised, multiphonon inelastic events become much more likely, depleting intensity from the elastic and single-phonon beams. However, by using the time-of-flight feature of the high-resolution instrument, one can simultaneously measure the attenuation of the elastically scattered He and the relative growth of the multiphonon processes.

In this short paper we present preliminary data on the surface dynamics of NaCl. Previously, the Rayleigh surface phonon mode had been reported in $\overline{\Gamma}\overline{M}$ of the surface Brillouin zone. We present data in this region which show the Rayleigh mode, a longitudinal resonance, a crossing mode and possibly additional features. These data are compared with the Green's function calculations of Benedek and co-workers and with the slab dynamics calculations of de Wette and co-workers. Further, we present arrival time spectra at several crystal temperatures which show the decrease in the specular beam and the relative growth of a multiphonon "foot" as the temperature is increased. A simple analysis of these data gives the average number of phonons exchanged per collision.

II. EXPERIMENTAL: HIGH-RESOLUTION He ATOM/SURFACE SCATTERING INSTRUMENT

The high-resolution He atom/surface scattering instrument has been described previously.[6] Briefly, the instrument is an ultrahigh vacuum (UHV) system consisting of several chambers connected together. The axis of the incident He atom beam and the axis of the detector intersect at the crystal with the fixed angle of 90°. This means that as the crystal is rotated about an axis perpendicular to the plane containing the beam and detector axes, the incident and scattering angles of the detected He atoms, θ_i and θ_f, measured with respect to the crystal surface normal, must satisfy $\theta_i + \theta_f = 90°$.

The He beam source consists of a high-pressure nozzle with a 30 μm diameter. In these experiments the nozzle tem-

peratures and pressures were varied to produce nearly monoenergetic beams ($\Delta E/E \simeq 2\%$) with incident wave vectors k_i ranging from ~ 7 to 9 Å^{-1} and energies $E_i = \hbar^2 k_i^2/2m$ from ~ 25 to 40 meV. We estimate that the beam has a cross sectional area of about 5 mm^2 at the crystal surface. A chopper disk with four slits is used to produce the pulsed He atom beam: the pulse widths are 7 μs; the pulse rate is typically 320 Hz.

The crystal is mounted on a manipulator which allows it to be oriented in the proper scattering plane, and heated and cooled over the range of ~ 110–1200 K. The incident angle θ_i (and hence, also the scattering angle θ_f) in these experiments can be varied by rotating the crystal on the manipulator with a stepping motor. A time-of-flight (TOF) technique is used to determine the speed and thus the wave vector and energy of the scattered He atoms. The flight path from the crystal to the detector entrance is 1060 mm. This length was chosen to keep the uncertainty introduced by the electron bombardment ionizer to less than 1%, since its length is about 10 mm. The He atom detector is a quadrupole mass spectrometer with a channeltron electron multiplier operated in the pulse counting mode. Data collection is automated by means of a CAMAC crate under computer control.

The NaCl crystal has fcc structure with a nonprimitive cell lattice spacing of 5.64 Å.[15] On the surface the primitive unit mesh is square with a lattice spacing 5.64 Å/$\sqrt{2}$ = 3.99 Å. A target sample was prepared by cleaving a large crystal in air [the natural cleavage plane is (001)] and then quickly placing a rectangular piece of the proper size (roughly 5 mm × 8 mm × 2 mm) onto the holder and inserting that onto the manipulator. The scattering chamber was then pumped down and baked at about 425 K for approximately 24 h. The crystal during this time was maintained at about 525 K. After the baking the crystal was flashed to about 775 K and then aligned.

In the experiments to determine the surface dispersion curves, namely the single-phonon scattering experiments, the crystal temperatures were kept at ~ 115 K. To prevent any physisorption problems, the crystal was routinely flashed every 24 h to ~ 775 K for a few minutes. No evidence of physisorption was ever observed, however.

III. RESULTS AND DISCUSSION

A. Angular distributions

Angular distribution experiments are performed by translating the chopper out of the beam so that one can measure the full scattered beam intensity as a function of angle θ_i. Figure 1 shows an angular distribution for NaCl in the ⟨100⟩ direction. The upper panel shows the Bragg (elastic) diffraction peaks, while the lower panel has the ordinate scale expanded by a factor of 100 to show the inelastic and bound-state resonance structure in the scattering. The condition for Bragg scattering is that[16]

$$\Delta \mathbf{K} = \mathbf{K}_f - \mathbf{K}_i = \mathbf{G}, \tag{1}$$

where $\mathbf{K}_i$ and $\mathbf{K}_f$ are the surface projections of the incident and final He atom wave vectors $\mathbf{k}_i$ and $\mathbf{k}_f$, respectively, and $\mathbf{G}$ is a surface reciprocal lattice vector. $K_i = k_i \sin\theta_i$ and

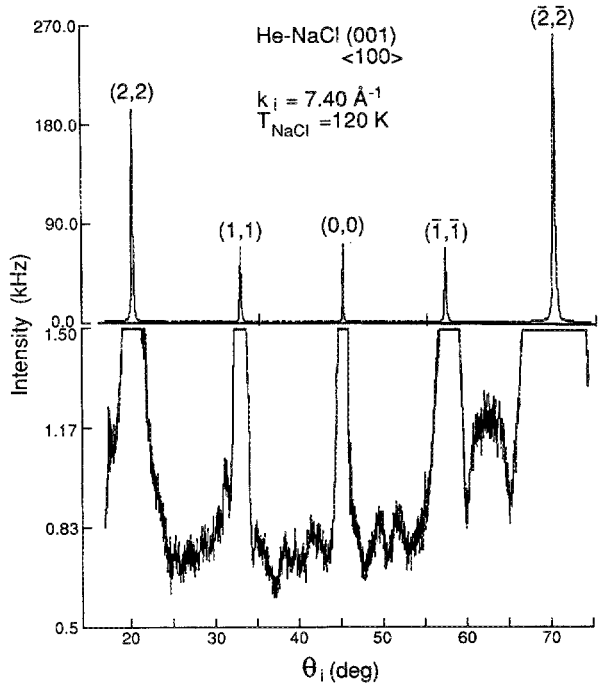

FIG. 1. Angular distribution for the NaCl (001) surface in the ⟨100⟩ direction. The lower panel has had the ordinate scale expanded by a factor of 100. The intensities are given in kHz.

$K_f = k_f \sin\theta_f = k_f \cos\theta_i$ for our 90° instrument geometry; for elastic scattering $k_f = k_i$.

For our purposes here the angular distributions are important for verifying the condition and the azimuthal alignment of the crystal surface. From Eq. (1) one can use the measured angular positions of the Bragg peaks to calculate the values of the reciprocal lattice vectors G_{nn}. One finds that the spacing in this direction (G_{11}) is 2.21 Å^{-1} compared with 2.23 Å^{-1} that is calculated from the bulk lattice spacing (given above, determined by other techniques). This means that this surface does not appear to reconstruct, just as is found with the other alkali halides. The widths of the Bragg peaks are also very narrow, $\sim 0.1°$, in agreement with that expected from the apparatus slit geometry.[6]

We defer discussion of the inelastic features of Fig. 1 to another paper.

B. Time-of-flight spectra; surface dispersion curves

The requirements for single-phonon annihilation or creation modify the scattering conditions of Eq. (1) to[16]

$$\Delta \mathbf{K} = \mathbf{K}_f - \mathbf{K}_i = \mathbf{G} + \mathbf{Q}, \tag{2}$$

where $\mathbf{Q}$ is the surface projection of the phonon wave vector. In addition, energy conservation requires that the phonon energy

$$\hbar\omega = E_f - E_i = \hbar^2(k_f^2 - k_i^2)/2m, \tag{3}$$

where a positive value for ω means that a phonon has been annihilated and a negative value means that one has been created in a single He scattering event. Thus, in a TOF measurement at angle θ_i, from the arrival time for a peak in the spectrum and the crystal-detector distance, one can calculate the k_f and K_f values needed to find ω and Q, and hence

the dispersion curve $\omega(\mathbf{Q})$.

Figure 2 shows a series of TOF spectra taken at several angles. Generally, the largest peaks are due to creation or annihilation of the Rayleigh wave phonons (the lowest lying sagittal-plane mode vibrations) which are marked with an *R*. In several of these spectra one sees also a diffuse elastic peak (marked *E*). These peaks violate Eq. (1) and are due to a small amount of disorder or defects on the surface. In several of the panels one can also find peaks that lie at longer (shorter) times than the Rayleigh mode positions. These are due to the creation (annihilation) of phonons which have greater energy than the Rayleigh wave and are labeled *C* for the crossing mode or *L* for the longitudinal mode, depending how near they lie to the calculated curves shown in Fig. 3. There are a few points labeled *U* which seem to lie in between and are uncertain. In a couple of spectra at angles near the first Bragg peak, $G_{\bar{1}\bar{1}}$, one can also see peaks labeled *D* between the elastic and the Rayleigh mode. These have been dubbed "deceptons" and are due to Bragg diffraction of the atoms with speeds in the small tail of the beam velocity distribution.[1]

Our experimental values for $\omega(\mathbf{Q})$ are plotted in Fig. 3 on the calculated dispersion curves for $\bar{\Gamma}\bar{M}$ by Benedek and Miglio[11] and in Fig. 4 on the calculated dispersion curves by

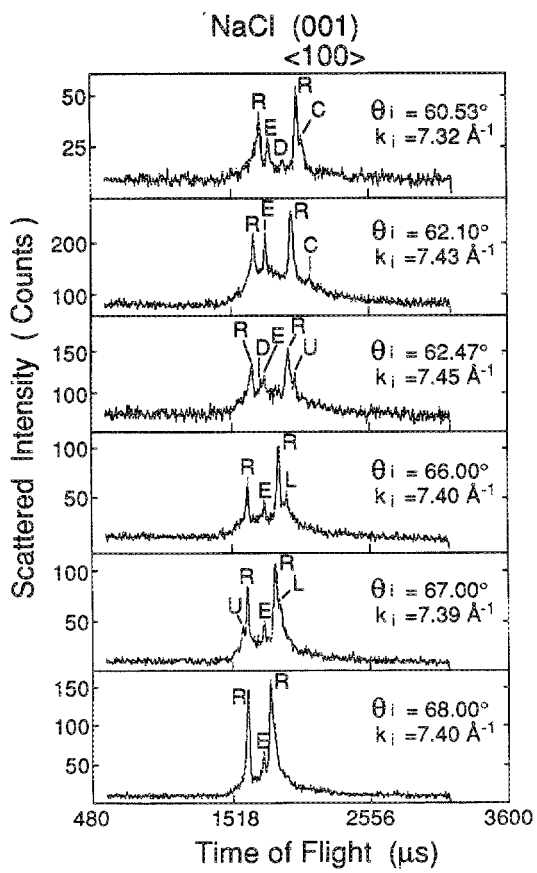

FIG. 2. Representative series of time-of-flight spectra of inelastically scattered He atoms from NaCl (001) in the (100) direction at several incident angles θ_i. The labelling of the observed peaks is based on their location relative to the calculation by Benedek and Miglio (Ref. 11) shown in Fig. 3. The letter designation is as follows: *E*, diffuse elastic peak; *R*, Rayleigh mode; *L*, longitudinal resonance; *C*, crossing mode (S_8); *U*, uncertain; *D*, deception.

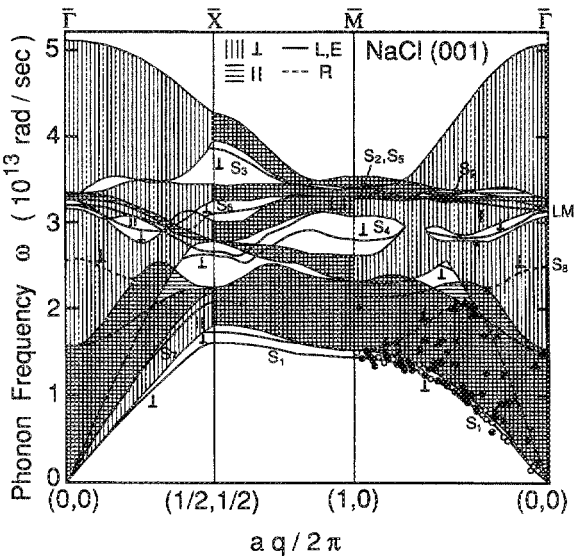

FIG. 3. Surface phonon dispersion curves for NaCl (001) over the $\bar{\Gamma}\bar{M}$ region of the surface Brillouin zone. The measured values from this work are indicated by the closed circles, except for closed triangles for those points with relatively weaker intensities. The open circles are from a previous investigation (Ref. 4). The Green's function calculation is taken from Benedek and Miglio. (Ref. 11).

Chen *et al.*[8] In general the agreement is quite good for the Rayleigh mode, S_1; there are several points very near the longitudinal resonance and the crossing mode labelled S_8 in Fig. 3. It is possible that the weak, high-lying point is associated with the Lucas mode in the gap or possibly with the bulk modes. We seem to have, in addition, some other points which lie between S_1, S_8, and the longitudinal resonance that are well resolved in the TOF. What these are due to we cannot be sure of at this time, again perhaps some feature in the bulk which couples relatively strongly to the He probe. The calculations shown in Fig. 4 give higher-frequency surface modes than those in Fig. 3 so that the agreement is not as good; however, the general shapes of the curves match the data fairly well.

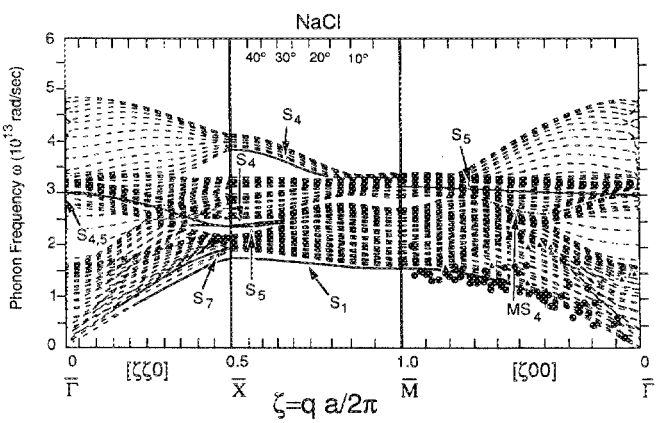

FIG. 4. Surface phonon dispersion curves for NaCl (001) over the $\bar{\Gamma}\bar{M}$ region of the surface Brillouin zone. The measured values are shown as in Fig. 3. The slab dynamics calculation is taken from Chen *et al.* (Ref. 8).

C. Temperature variation of the crystal; multiphonon scattering

Figure 5 shows a series of TOF spectra for a range of crystal temperatures taken at $\theta_i = 45°$. As the temperature is raised, the specular beam intensity falls and a "foot" appears to grow around the base of it.

We give here a very brief summary of a model for the intensity of the diffuse inelastic scattering to be published elsewhere.[17] The intensity for elastic scattering with reciprocal lattice vector **G** can be written in the (approximate) form

$$I_G = I_G(0)e^{\ 2W} = I_G(0)e^{-\alpha T}. \tag{4}$$

Inelastic processes are also governed by a similar Debye-Waller functional form

$$I_{\text{inel}} = I_0 e^{-2W}(A_0 + A_1 T + A_2 T^2 + \cdots), \tag{5}$$

where I_0 is the low temperature inelastic scattering intensity and where each term in the power series corresponds to a particular order of phonon exchange; that is, to the average number of phonons exchanged. Equations (4) and (5) suggest that one can find the polynomial in a plot of I_{inel}/I_G as a function of T since

$$I_{\text{inel}}/I_G = (\text{const})(A_0 + A_1 T + A_2 T^2 + \cdots). \tag{6}$$

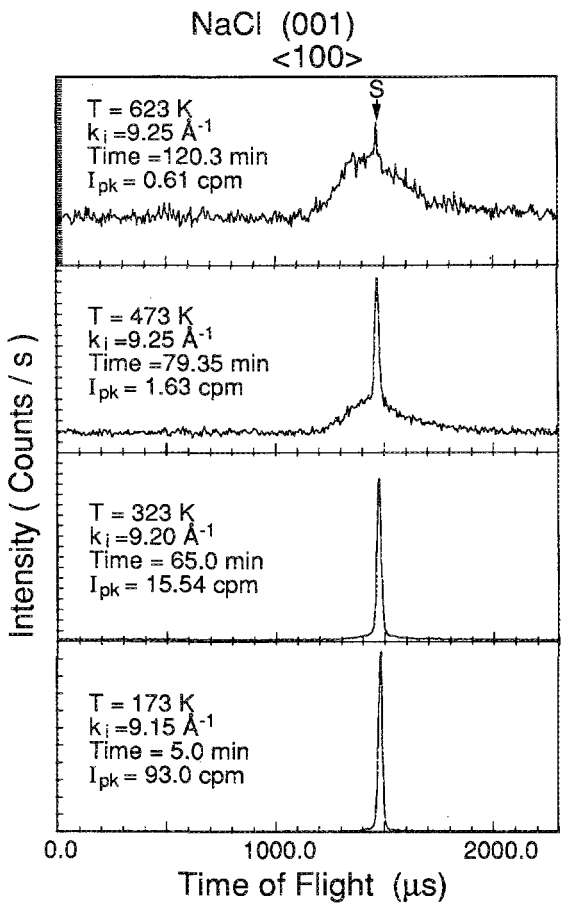

FIG. 5. A representative series of time-of-flight spectra taken at 45° to show the relative growth of the inelastic foot compared to the specular beam with crystal temperature T. The incident wave vector k_i given in each panel has units of Å^{-1}; the peak height in each spectrum (I_{pk}) is the count rate in counts per minute; the total accumulation time for each spectrum is given in minutes. The flight times on the abscissa are in μs. In the top panel an arrow marks the position of the specular beam.

Figure 6 shows a semilog plot for the peak of the inelastic scattering intensity at the base of the specular peak G_{00} (the specular intensity is removed) versus T. Over the temperature range of about 350 to 670 K the plot gives a fairly good straight line with a slope of 0.014. That is, we find an approximately exponential temperature dependence in this range. To correspond to the model, we note that $e^{\beta T} = \Sigma(\beta T)^n/n!$. The greatest term in the series is the one with $n = \beta T = N_{\max}$ and the number of important terms is approximately $2N_{\max}$. Thus, from our data $N_{\max} = 7$ at 500 K. This model, then, implies that phonon exchanges of ~5–9 are typical in the temperature range we studied and exchanges of up to ~10–18 phonons are non-neligible. In similar experiments with NaI the values obtained for phonon orders were about twice as large.[18] This is consistent with the lower vibrational frequencies for NaI as, for example, the Rayleigh wave frequencies for NaI are only about half as large as those for NaCl at corresponding points in the Brillouin zone.[18]

IV. CONCLUSIONS

We can summarize the results of these preliminary measurements in the following.

(1) High-resolution He atom scattering experiments are capable of providing the surface dispersion curves from the zone center to the edge of the surface Brillouin zone for the Rayleigh mode and for some higher-lying longitudinal acoustic and optical modes.

(2) The calculations based on the shell models which use parameters obtained by fitting the bulk dispersion curves seem to give generally good agreement with the experimental results. In particular, the experiments appear to confirm the existence of a crossing mode in NaCl which is predicted by the calculations.[19] Implicitly, the good agreement between the calculations and the experiments justifies the neglect of relaxation in the calculations. In more recent slab dynamics calculations which take into account the relaxation in NaCl, the same conclusion is reached.[20]

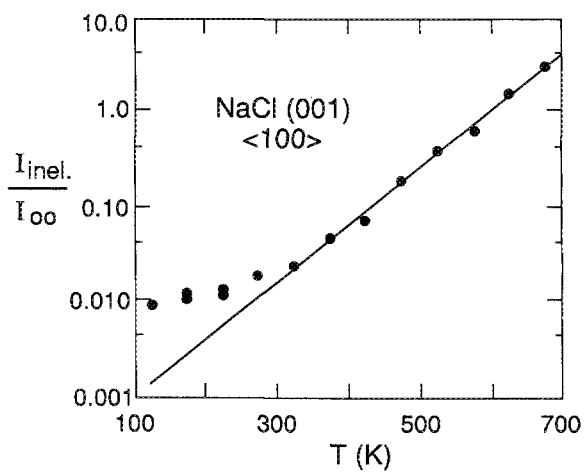

FIG. 6. A semilog plot of the inelastic scattering intensity divided by the specular beam intensity vs temperature. The inelastic maxima and elastic intensities were taken directed from the time-of-flight spectra. A linear least squares fit was used to find the slope for the data above 300 K.

(3) High-resolution He atom scattering is able to provide a direct probe of the multiphonon interactions. From the simple model analysis of the data one may conclude that collision models must include contributions from terms that describe relatively large numbers of phonons exchanged.

Further experiments on this crystal are being carried out in the $\bar{\Gamma}\bar{X}$ part of the surface Brillouin zone to map out the surface dispersion relations as completely as possible. Based on the calculations, one expects again to observe the Rayleigh mode, a longitudinal acoustic mode and a crossing mode. However, it may also be possible to obtain better data on the Lucas mode. Additional experiments will also be carried out on the multiphonon scattering to investigate the model more thoroughly, in particular the temperature variation of the "foot" width.

ACKNOWLEDGMENTS

The authors from FSU gratefully acknowledge support from the U.S. Department of Energy under Grant No. DE-FG05-85ER45208. We also gratefully acknowledge assistance with some of the calculations by G. Bishop.

[1] G. Brusdeylins, R. B. Doak, and J. P. Toennies, Phys. Rev. B **27**, 3662 (1983).
[2] G. Bracco, R. Tatarek, S. Terreni, and F. Tommasini, Phys. Rev. B **34**, 904 (1986).
[3] G. Benedek, G. Brusdeylins, L. Miglio, R. Rechsteiner, J. G. Skofronick, and J. P. Toennies, Phys. Rev. B **28**, 2104 (1983).
[4] G. Benedek, G. Brusdeylins, R. B. Doak, J. G. Skofronick, and J. P. Toennies, Phys. Rev. B **28**, 2104 (1983).
[5] G. Chern, W. P. Brug, S. A. Safron, and J. G. Skofronick, J. Vac. Sci. Technol. A **7**, 2094 (1989).
[6] G. Chern, J. G. Skofronick, W. P. Brug, and S. A. Safron, Phys. Rev. B **39**, 12828 (1989).
[7] G. Chern, J. G. Skofronick, W. P. Brug, and S. A. Safron, Phys. Rev. B **39**, 12838 (1989).
[8] T. S. Chen, F. W. de Wette, and G. P. Alldredge, Phys. Rev. B **15**, 1167 (1977).
[9] W. Kress, F. W. de Wette, A. D. Kulkarni, and U. Schroeder, Phys. Rev. B **35**, 5783 (1987).
[10] G. Benedek, Surf. Sci. **61**, 603 (1976).
[11] G. Benedek and L. Miglio, in *Ab Initio Calculations of Phonon Spectra*, edited by J. Devreese, V. E. van Doren, and P. E. van Camp (Plenum, New York, 1982).
[12] R. Reiger, J. Prade, U. Schroeder, F. W. de Wette, A. D. Kulkarni, and W. Kress, Phys. Rev. B **39**, 7938 (1989).
[13] See solid-state physics texts, for example, W. A. Harrison, *Solid State Theory* (Dover, New York, 1980), p. 426.
[14] R. Manson and V. Celli, Surf. Sci. **24**, 495 (1971).
[15] R. W. G. Wyckoff, *Crystal Structures* (Wiley, New York, 1964), Vol. 1.
[16] For example, see G. Boato and P. Cantini, Adv. Electron. Electron Phys. **60**, 95 (1983).
[17] J. R. Manson (unpublished).
[18] G. Chern, J. Duan, J. G. Skofronick, W. P. Brug, and S. A. Safron (unpublished).
[19] The first prediction was in the Green's function calculation by G. Benedek, Phys. Status Solidi B **58**, 661 (1973).
[20] F. W. de Wette, W. Kress, and U. Schroeder, Phys. Rev. B **32**, 4143 (1985).